energyequipsys/ Vol 4/No2/Dec 2016/ 225-244

ENERGY EQUIPSYS

Energy Equipment and Systems

http://energyequipsys.ut.ac.ir
www.energyeuquipsys.com

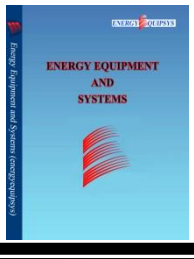

Exergo-environmental and exergo-economic analyses and multi-criteria optimization of a novel solar-driven CCHP based on Kalina cycle

Authors

Mona Rahmatian[a]
Fateme Ahmadi Boyaghchi [a*]

[a] Department of Mechanical Engineering, Faculty of Engineering & Technology, Alzahra University, Tehran, Iran

ABSTRACT

The present research proposes and optimizes the performance of a novel solar-driven combined cooling, heating, and power (CCHP) Kalina system for two seasons—winter and summer—based on exergy, exergo-economic, and exergo-environmental concepts applying a Non-dominated Sort Genetic Algorithm-II (NSGA-II) technique. Three criteria, i.e. daily exergy efficiency, total product cost rate, and total product environmental impact rate associated with the exergy of the system for each season are considered simultaneously for multi-objective optimization. The outcomes reveal that increments in turbine inlet pressure and mass flow rate of the vapour generator lower the environmental impact of system products as well as the total product cost rate in both seasons. The optimum value of daily exergy efficiency, total product environmental impact rate, and total product cost rate indicate improvements by 2.56%, 15.7%, and 15.3% respectively in summer and 36.34%, 7.39%, and 4.93% respectively in winter, relative to the base point.

Article history:

Received : 14 May 2016
Accepted : 14 August 2016

Keywords: CCHP, Exergy Analysis, Exergo-Economic Analysis, Exergo-Environmental Analysis, Multi-Objective Optimization.

1. Introduction

The Kalina cycle is a thermodynamic cycle to convert thermal energy into mechanical power. It does this by using working fluid with at least two different components, such as ammonia-water, and a varied ratio between those components in different parts of the system, which helps increase thermodynamic reversibility, and therefore, also thermodynamic efficiency. Russian engineer Alexander Kalina [1] invented the Kalina cycle. P K Nag et al. [2] analyzed the Kalina cycle with reference to both the first and the second laws, providing a rational procedure to estimate the NH_3-H_2O mixture properties. They used Kalina cycle to reduce thermal irreversibility of the thermodynamic cycle. Xinxin Zhang in 2012 [3] researched on the Kalina cycle. That paper presented a review of the research on Kalina cycle, including its description, a comparison of the Rankine and Kalina cycles, energy and exergy analyses of the Kalina cycle, different Kalina systems, and their different applications.

Many papers have described the characteristics of the Kalina cycle. For a special case of geothermal applications in 1989, Kalian and Leibowitz [4] analyzed the Kalian cycle thermodynamically, with a geothermal heat source. Madhawa

*Corresponding author: Fateme Ahmadi Boyaghchi
Address: Department of Mechanical Engineering, Faculty of Engineering & Technology, Alzahra University, Tehran, Iran
E-mail address: fahmadi@alzahra.ac.ir

Hettiarachchi et al. [5] evaluated the performance of the Kalina cycle system with low-temperature geothermal heat sources. They compared it with an organic Rankine cycle, and examined the effect of the ammonia fraction and turbine inlet pressure on the cycle performance. Nasruddin et al. [6] determined the energy and exergy analyses of the Kalina cycle with lower temperature geothermal resources, and optimized it based on the mass fraction of working fluid and the turbine output pressure. In 2009, P A Lolos [7] investigated a Kalina cycle using low-temperature heat sources to produce power. The main heat source of the cycle was provided from flat solar collectors. In addition, an external heat source was connected to the cycle, which corresponds to 5–10% of the total thermal energy supplied to the cycle. The NH_3 mass fraction at the turbine inlet varied along with the expansion pressure, and the effects on the cycle efficiency were studied. For given conditions, an optimum range of vapour mass fractions and operating pressures could be identified, resulting in optimum cycle performance. Faming Sun et al. [8] studied a solar-boosted Kalina system with an auxiliary super heater. The main heat source of the cycle was provided by flat-plate solar collectors. N Shankar et al. [9] investigated a low-temperature Kalina cycle to optimize the heat recovery from solar thermal collectors. Jiangfeng Wang et al. [10] simulated a solar-driven Kalina cycle to utilize solar energy effectively by using ammonia-water's varied-temperature vaporizing characteristics. They optimized the Kalina cycle with a genetic algorithm to maximize its thermal efficiency. In 2013, Xinguo Li et al. [11] evaluated a Kalina cycle with an ejector (EKalina cycle). The ejector was used to substitute the throttle valve and the absorber in the Kalina cycle system 11 (KCS 11).

Studies on the cogeneration system (combined power and cooling) with ammonia-water as the working fluid, with respect to exergy and exergo-economic concepts, have recently gained considerable attention. In 2000, Feng Xu et al. [12] studied a combined thermal power and cooling cycle based on thermodynamic analysis. It can provide power output as well as refrigeration, with power generation as the primary goal. This cycle uses an absorption condensation process different from the conventional one. This paper presents a parametric analysis of the proposed cycle. A novel cogeneration proposed by Goswami is under intensive investigation, both theoretically and experimentally [13, 14]. The first and second laws of thermodynamics were used to analyze a novel thermodynamic cycle proposed by Goswami which uses an ammonia-water binary mixture as the working fluid, while producing both power and cooling [15, 16]. C P Jawahar et al. [17] simulated a GAX-based Kalina cycle for both power and cooling applications. They studied the effects of various parameters like heat source temperature, refrigeration temperature, sink temperature, split ratio (refrigerant flow ratio between power and cooling systems), split factor (solution flow ratio between absorber and GAX heat exchanger) on the performance of the cycle. V Zare et al. [18] investigated the performance of an ammonia-water power/cooling cogeneration cycle, carried out thermo-economic analysis, and optimized this system. S Ma et al. [19] proposed and modelled a new CCHP system thermodynamically driven by solid oxide fuel cell based on ammonia-water mixture to recover the waste heat of the exhaust from the solid oxide fuel cell combined with a gas turbine to enhance energy conversion efficiency as well as to reduce the emission of greenhouse gases and pollutants. The application of two absorbers in the proposed cycle produces the cooling effect.

Besides the exergy and exergo-economic methods, and the exergo-environmental analysis, a combination of exergy analysis and lifecycle assessment (LCA) principles is a relatively new method to evaluate the environmental impacts of energy conversion systems. Some of these systems are the high-temperature solid oxide fuel cell [20], the vapour methane reform process for hydrogen production [21], the oxy-fuel power plant with and without CO_2 capture [22, 23], the turboprob engine used in district airplanes [24], the traditional coal boiler, the condensing natural gas-fired combi boiler [25], the reverse osmosis seawater purification plant [26], the hybrid electrical vehicle thermal direction system [27], the gas-fired steam power plant [28], the geothermal district heating system [29], the cogeneration system based on an organic Rankine cycle used in the cement industry [30], and an air-conditioning system [31].

To the best of the researchers' knowledge, no research has been done on the assessment and multi-criteria optimization of a solar-driven CCHP Kalina cycle based on the

exergo- environmental concept. The present work proposes and models a novel solar-driven CCHP Kalina cycle integrated with parabolic trough solar collectors based on the ejector refrigeration cycle with respect to exergy, exergo-economic and exergo-environmental principles for two modes, i.e. summer and winter, for the first time. The desired system will then be optimized by maximizing the daily exergetic efficiency, and minimizing the total product cost rate and the total product environmental impact associated with the exergy rate. Six main parameters were selected as decision variables for summer, and five for winter. The NSGA-II technique was applied to provide the optimum solutions for each season.

Nomenclature

A_{coll}	Solar collector area (m^2)
ex	Specific exergy (kJ/kg)
$\dot{Ex}$	Exergy (KW)
G_t	Total instantaneous radiation, W/m^2
h	Specific enthalpy (kJ/kg)
i	Inlet
$\dot{m}$	Mass Flow Rate (kg/s)
e	Outlet
P	Pressure
$\dot{Q}$	Heat transfer rate (KW)
R	Gas constant (kJ/kg K)
s	Specific Entropy (Kj/KgK)
T	Temperature (°C)
$\dot{W}$	Power (kW)
x_k	Number of molecules of gas k (molecules)

Subscripts

0	Ambient
ch	Chemical
D	Destruction
elec	Electrical
Eva	Evaporator
Gen	Generator
HHV	High Heating Value
ph	Physical
D	Destruction
elec	Electrical
Eva	Evaporator
Gen	Generator
HHV	High Heating Value
ph	Physical
Turb	Turbine

Greek symbols

ε	Exergy efficiency

Abbreviation

EES	Engineering Equation Solver
ORC	Organic Rankine Cycle

2.System Description

The proposed CCHP system driven by solar energy consists of two subsystems, namely, the solar subsystem and the CCHP Kalina subsystem, as Fig. 1 shows.

The solar subsystem includes the parabolic trough solar collector (PTC) field, a thermal storage tank, and an auxiliary heater. A thermal storage tank is applied to correct the mismatch between the supply of the solar energy and the demand for thermal source consumed by the CCHP Kalina subsystem. Thus, the system could act stably and continuously. The auxiliary heater is activated to elevate and fix the outlet temperature of the thermal storage tank. The heat-transfer medium in the solar subsystem is Therminol VP-1 for its large heat capacity.

The CCHP subsystem, combining a Kalina cycle with an ejector refrigeration cycle, is made up of a vapour generator, a turbine, an evaporator, a heater, a condenser, a low-temperature (LH) recuperator, a high-temperature (HP) recuperator, a throttle valve, an ejector, a pump, two regulation valves, and several mixers. The ammonia-water mixture is applied as working fluid to absorb the heat from the Therminol VP-1 in the vapour regenerator to produce an ammonia-water vapour-liquid mixture. The ammonia-rich saturated vapour coming from the separator is expanded by the extraction turbine to generate electricity. In the summer mode, the stream extracted from the turbine flows into the ejector as a primary flow to suck the secondary flow from the evaporator with very low pressure. Then, the primary flow and the secondary flow are mixed to ensure that a mid-pressure flow leaves the ejector. The ammonia-lean saturated liquid leaving the separator is mixed with the turbine exhaust after heating an ammonia-water basic solution in the HT recuperator. It is then mixed with the third stream from the ejector after releasing heat into the stream flowing into the vapour generator in the LT recuperator. The mixed streams are then delivered to a condenser to condense the working fluid by releasing the heat into the environment. The

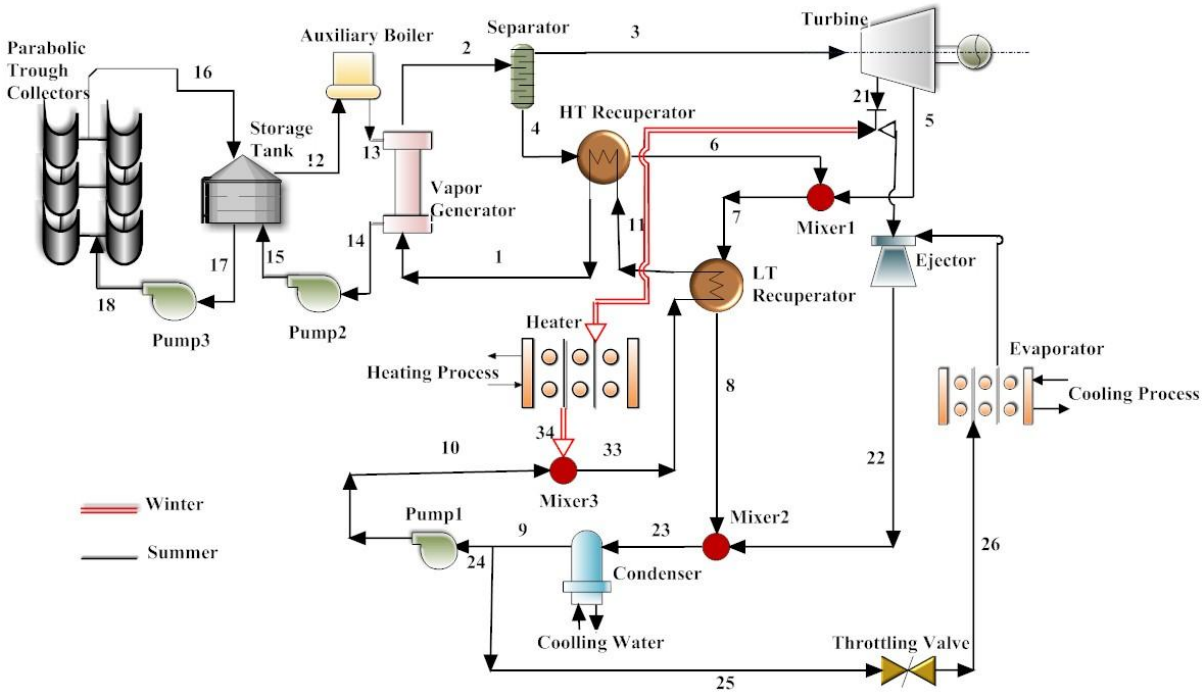

Fig.1. A schematic diagram of the solar-driven CCHP Kalina system

liquid working fluid is also divided into two streams. One is throttled down to a very low pressure through a throttle valve and vaporized in an evaporator by absorbing heat to produce a cooling effect. The other stream is pumped up to a high pressure and delivered back to the vapour generator. In the winter mode, the extracted stream from the turbine flows into the heater instead of the ejector to provide the users with heat energy. It is then mixed with the stream coming from the pump.

3.Methodology

3.1.PTC model

The PTC can accept beam radiation, Gb. The beam radiation flux falling on the aperture surface of the plane is calculated as follows [32]

$$G_b = G - G_d \quad (1)$$

where G and Gd are the total and diffused radiation determined by:

$$G = \frac{\pi}{24}\left(\frac{\cos(hh)-\cos(hss)}{\sin(hss)-\left(\frac{2\pi \times hss}{360}\right)\cos(hss)}\right)\left(\frac{\bar{H}}{3600}\right)(\alpha+\beta\cos(hh)) \quad (2)$$

$$\alpha = 0.409+(0.5016\times\sin(hss - 60)) \quad (3)$$

$$\beta = 0.6609+(0.4767\times\sin(hss - 60)) \quad (4)$$

In Eq. (2), hh, hss and $\bar{H}$ are hour angle, sunset hour angle, and monthly averaged total insolation incident on a horizontal surface respectively. The diffuse radiation is calculated as [32]:

$$G_d = \frac{\pi}{24}\left(\frac{\cos(hh)-\cos(hss)}{\sin(hss)-\left(\frac{2\pi \times hss}{360}\right)\cos(hss)}\right)\left(\frac{\bar{H}_d}{3600}\right) \quad (5)$$

where $\bar{H}_d$ is the monthly averaged daily diffuse radiation on a horizontal surface [32]. The energy gain of PTC can be calculated as follows [32].

$$Q_u = n\times(G_b\times\eta_{optical}\times A_{ap}) - (A_r\times U_L(T_r - T_a)) \quad (6)$$

where n, $\eta_{optical}$, indicates the number of collectors and the optical efficiency. A_{ap} is the aperture area and Tr, Ar, and Ta are the receiver temperature, the receiver area, and the ambient temperature respectively.

In Eq. (6), the heat transfer coefficient, UL, based on the receiver area, Ar, is given by [32]:

$$\frac{1}{U_L} = \left[\frac{A_r}{(h_w + h_{ca})A_c} + \frac{1}{h_{rc}}\right] \quad (7)$$

where Ac is the external area of glass cover;

'hw' expresses the convection heat transfer coefficient from cover to ambient; hca and hcr are the linearized radiation coefficient from the cover and ambient, and the linearized radiation coefficient from the receiver to cover respectively, as estimated by Eqs. (8) and (9) [32]:

$$h_{ca}=\sigma.\varepsilon_c.(T_c+T_a)(T_c^2+T_a^2) \quad (8)$$

$$h_{rc}=\frac{\sigma\,(T_c+T_r)(T_c^2+T_r^2)}{\frac{1}{\varepsilon_r}+\frac{A_r}{A_c}(\frac{1}{\varepsilon_c}-1)} \quad (9)$$

3.2.Thermal storage tank model

A thermal storage tank is mounted to operate as a buffer between the PTC and the bottom CCHP Kalina subsystem. The tank is assumed to be insulated and the oil to be well mixed so that the oil temperature TL varies only with time. The following equation can be obtained from the energy balance in the tank [33].

$$\left[\left(\rho VC_p\right)_{Oil}+\left(\rho VC_p\right)_{ST}\right]\frac{dT_{Oil}}{dt} = Q_u-Q_{load}-\left(UA\right)_{ST}\left(T_{Oil}-T_a\right) \quad (10)$$

where the Qload, representing the energy discharged to *the* CCHP Kalina subsystem, can be calculated as:

$$Q_{load}=m_{oil}C_p\left(T_{Oil}-T_i\right) \quad (11)$$

3.3.CCHP model

In the present study, some assumptions were made to simplify the analysis of CCHP:

1. The system operate*d* in a steady state condition.
2. The pressure drop in the heat exchangers and connection pipes were neglected.
3. The vapour and liquid streams leaving the separator were saturated.
4. The throttling process was isenthalpic.
5. The pumps and ammonia-water turbine had a given isentropic efficiency.
6. The velocities at the inlet and outlet of the ejector were neglected.
7. The constant-pressure model was applied to the modelling ejector [34].
8. The motive and suction streams reached the same pressure at the inlet of the constant - area mixing section of the ejector, and no mixing occurred between the two streams before the inlet of the mixing section [34].
9. The friction losses in the ejector were considered in terms of the efficiencies of the nozzles, the mixing section, and the diffuser [34, 35].
10. The flow at the ejector was steady and one-dimensional [34, 35].
11. Each component was considered as a control volume with corresponding inlet and outlet streams.

The mass, energy conservation, and the concentration balance applied for each component are as follows [36]:

$$\Delta_{out}^{in}\sum\dot{m}=0 \quad (12)$$

$$\dot{Q}-\dot{W}=\Delta_{out}^{in}\sum\dot{m}h \quad (13)$$

$$\Delta_{out}^{in}\sum\dot{m}x=0 \quad (14)$$

3.4.Exergy analysis

Exergy analysis is a tool to help a user analyse the energy use. Thus, it is useful to gain better efficiency [33]. Exergy is represented in four terms, but in this study, kinetic and potential exergies are neglected.

$$ex_k=(h_k-h_0)-T_0(s_k-s_0) \quad (15)$$

In this research, the ammonia-water at 5°C, 101.325 kPa with a concentration of 0.82 kg/kg are assumed to be a dead state [37]. Chemical exergy of oil in the collector subsystems is neglected.

The Fuel-Product-Loss method has been applied for exergy analysis. The fuel exergy rate (EX_F) and the product exergy rate (EX_P) are defined as a required input and a desired output respectively. The inefficiencies are measured by the exergy loss rate (EX_L) and the exergy destruction rate (EX_D). If the heat-transfer process happens at constant temperature for a component (Tk), the exergy loss is given by [33]:

$$\dot{E}x_{L,k}=\dot{Q}_{Loss}(1-\frac{T_o}{T_k}) \quad (16)$$

The exergy rate balance for each component of the desired system can be calculated by [33]:

$$\dot{E}x_{F,k}-\dot{E}x_{P,k}-\dot{E}x_{D,k}-\dot{E}x_{L,k}=0 \quad (17)$$

3.5.Exergoeconomic analysis

Thermo-economics is the branch of engineering that combines exergy analysis and economic principles to provide the system designer or operator with information not available through conventional energy analysis and economic evaluations but is crucial to the design and operation of a cost-effective system [33]. The thermo-economic balance of each component is carried out based on exergy and cost balances. In a conventional economic analysis, a cost balance is usually formulated for the overall system operating at a steady state as follows [33]:

$$\sum_{out} \dot{C} = \sum_{in} \dot{C} + \dot{Z} \quad (18)$$

$$\dot{C} = c.\dot{E}x \quad (19)$$

In Eq. (18), Z denotes capital investment and the operating and maintenance (O&M) cost rate. The cost rate of each component is calculated as [33]:

$$\dot{Z}_{K,in} = TCI \times CRF \quad (20)$$

where, CRF indicates a capital recovery factor determined as [33]:

$$CRF = \frac{i(1+i)^N}{(1+i)^N - 1} \quad (21)$$

$$TCI_k = 6.32 \times \dot{C}_{B,k} \quad (22)$$

where C_B is the cost rate in the base year (2013) obtained from the Marshal economic indicator [38].

The operating and maintenance cost rate of each component is taken as 25% of the equipment buying cost [33].

The fuel and O&M costs may vary considerably during the system's economic life. Therefore, the levelized annual cost should be calculated in the cost analysis. The levelized values of the fuel and O&M costs can be calculated by multiplying expenditures in the first year by the constant escalation levelization factor (CELF) [33]:

$$CELF = CRF \cdot \frac{k(1-k^N)}{1-k} \quad (23)$$

$$k = \frac{1+r_n}{1+i} \quad (24)$$

In Eq. (21), i is the interest rate and N is the system life. In Eq. (24), rn is the nominal escalation rate. Table 2 lists the values of cost parameters.

Table 1. Component costs

Component cost	Dependent variable	Cost ($)
Turbine	Turbine power, (kW)	$PEC_{Tur} = 4505 \times (\dot{W}_{Tur})^{0.7}$ [39, 40]
Heat exchangers (evaporator, vapour generator, condenser, heater, LT and HT recuperators)	Heat exchanger area (m2)	$PEC_{HE} = 3.28 \times 10^4 \times (\frac{A_{HE}}{80})^{0.68}$ [40]
Pump	Pump power (kW)	$PEC_{Pump} = 9.84 \times 10^3 (\frac{\dot{W}_P}{4})^{0.55}$ [40]
Storage tank	Tank volume (m3)	$PEC_{ST} = 1.15 \times 10^4 \times (\frac{V_{ST}}{5})^{0.53}$ [40]
PTC	Collector area (m2)	$PEC_{PTC} = A_{PTC} \times 250$ [41]
Auxiliary boiler	Steam mass rate	$PEC_{AB} = 4.64 \times 10^5 (\frac{SG_{AB}}{50000})^{0.96}$ [40]

Table 2. Cost parameters

Parameters	Value
Interest rate, i	12% (42)
System life, N	30 years (42)
Nominal Escalation rate, rn	5% (43)

3.6.Exergo-environmental analysis

The exergo-environmental analysis is considered to be one of the most promising tools to assess energy-conversion processes from an environmental point of view [20]. It is an appropriate combination of the exergy analysis and the LCA and provides information about the effect of thermodynamic inefficiency on environmental impacts.

Exergy analysis is a powerful tool to evaluate the quality of a resource as well as the location, magnitude, and causes of thermodynamic inefficiencies. LCA is a technique to assess the environmental impact associated with a product over its lifecycle. It can be assessed using an ECO-indicator 99. The standard ECO-indicator 99 supplies data for the production and processing of a lot of materials, for transport processes, for disposal scenarios, etc. In addition, LCA provides the environmental impacts of a component or an overall system during its life.

For the LCA of the system being analyzed, we assumed, in analogy with the economic analysis, a lifetime of 15 years, and 7,446 working hours per year at full capacity.

The exergo-environmental analysis for a system consists of environmental impact balances written for the k-th component and auxiliary equations based on the P and F rules [20]. The environmental impact balances can be written as [44]:

$$\dot{B}_{P,k} = \dot{B}_{F,k} + \left(\dot{Y}_k + \dot{B}_k^{PF}\right) \quad (25)$$

In Eq. (25), Y_k indicates the component-related environmental impact of component k, obtained by considering the entire lifecycle of the component, i.e. (a) construction, Y_k^{CO}, (including manufacturing, transport, and installation), (b) operation and maintenance, Y_k^{OM}, and (c) the disposal, Y_k^{DI}, of component k [44]:

$$\dot{Y}_k = \dot{Y}_k^{CO} + \dot{Y}_k^{OM} + \dot{Y}_k^{DI} \quad (26)$$

The environmental impact of exergy destruction $B_{D,k}$ identifies the environmental impact as a result of the exergy destruction within the k-th component [20]:

$$\dot{B}_{D,k} = b_{F,k}\dot{E}x_{D,k} \quad (27)$$

where bF,k is the environmental impact per unit of the exergy of the fuel provided to component k.

The exergo-environmental balance and the auxiliary equations for the system components in the current study are given in Tables 3-a and 3-b, for summer and winter respectively. The solution of this equation system allows us to find all the values of the environmental impact rate.

In Eq. (25), B_k^{PF} is the environmental impact of pollutant formation within the component defined only when a chemical reaction takes place; in any other case, it is zero [44]. For the components in which chemical reactions occur, the value of B_k^{PF} is calculated as follows:

$$\dot{B}_k^{PF} = \sum_i b_i(\dot{m}_{i,out} - \dot{m}_{i,in}) \quad (28)$$

where only pollutant streams that will be emitted to the environment—i.e. CO, CO_2, CH_4, N_2O, NO_x, and SO_x—are taken into account [20].

In an auxiliary boiler, the exergo-environmental balance can be written as:

$$\dot{B}_{12} + \dot{B}_f + \dot{Y}_{AB} = \dot{B}_{13} \quad (29)$$

where B_f is the exergo-environmental impact of natural gas (NG) calculated as:

$$\dot{B}_f = b_f \times \dot{E}x_{NG} \quad (30)$$

The environmental impact of the natural gas stream (bf) consists of the sum of the environmental impact of CH_4 as a reactant and the environmental impact of CH_4 as a pollutant. Therefore,

$$b_f = \frac{(b_{CH_4} + b_{CH_4}^{pf}) \times \dot{m}_{NG}}{\dot{Ex}_{NG}} \quad (31)$$

Here, the values of b_{CH_4} and $b_{CH_4}^{Pf}$ are set at 0.265 and 0.114 respectively [45].

4.Performance criteria

Three performance parameters, viz. daily exergetic efficiencies, the total product cost rate, and the total product environmental impact rate, are defined to assess the overall system.

4.1.Daily exergy efficiency

The daily exergy efficiencies of the overall system for each season can be expressed as [46]:

$$\eta_{ex,summer} = \frac{\int\left(\dot{W}_{net} + \dot{E}x_{P,Evap}\right)d\tau}{\int\left(\dot{E}x_{AB} + \dot{E}x_{P,sun}\right)d\tau} \quad (32)$$

Table 1-a. Exergo-environmental balances and auxiliary equations for the system components in summer

Components	Exergo-environmental balance equations	Auxiliary equations
The CCHP subsystem		
Vapour generator	$\dot{B}_1+\dot{B}_{13}+\dot{Y}_{VG}=\dot{B}_2+\dot{B}_{14}$	$b_{13}=b_{14}$
Separator	$\dot{B}_2+\dot{Y}_{Sep}=\dot{B}_3+\dot{B}_4$	$\frac{\dot{B}_4-\dot{B}_2}{\dot{E}x_4-\dot{E}x_2}=\frac{\dot{B}_3-\dot{B}_2}{\dot{E}x_3-\dot{E}x_2}$
Turbine	$\dot{B}_3+\dot{Y}_{Tur}=\dot{B}_{21}+\dot{B}_5+\dot{B}_{w,Tur}$	$b_3=b_5=b_{21}$
HT Recuprator	$\dot{B}_4+\dot{B}_{11}+\dot{Y}_{HT}=\dot{B}_1+\dot{B}_6$	$b_1=b_{11}$
LT Recuprator	$\dot{B}_7+\dot{B}_{10}+\dot{Y}_{LT}=\dot{B}_8+\dot{B}_{11}$	$b_7=b_8$
Mixer1	$\dot{B}_5+\dot{B}_6+\dot{Y}_{Mxr1}=\dot{B}_7$	-
Pump1	$\dot{B}_{24}+\dot{B}_{w,Pump1}+\dot{Y}_{Pump1}=\dot{B}_{10}$	-
Mixer2	$\dot{B}_8+\dot{B}_{22}+\dot{Y}_{Mxr2}=\dot{B}_{23}$	-
Condenser	$\dot{B}_{23}+\dot{B}_{19}+\dot{Y}_{Con}=\dot{B}_9+\dot{B}_{20}$	$b_{23}=b_9$
Evaporator	$\dot{B}_{26}+\dot{B}_{28}+\dot{Y}_{Evap}=\dot{B}_{27}+\dot{B}_{29}$	$b_{26}=b_{27}$
Ejector	$\dot{B}_{27}+\dot{B}_{21}+\dot{Y}_{Ejc}=\dot{B}_{22}$	-
The temperature stabilization subsystem		
Storage tank	$\dot{B}_{15}+\dot{B}_{16}+\dot{Y}_{ST}=\dot{B}_{17}+\dot{B}_{12}+\dot{B}_L$	$b_{12}=b_{17}$
Pump2	$\dot{B}_{14}+\dot{B}_{w,Pump2}+\dot{Y}_{Pump2}=\dot{B}_{15}$	-
Auxiliary boiler	$\dot{B}_{12}+\dot{B}_f+\dot{Y}_{AB}=\dot{B}_{13}$	-
The solar collection subsystem		
PTC	$\dot{B}_{18}+\dot{B}_{sun}+\dot{Y}_{PTC}=\dot{B}_{16}$	-
Pump3	$\dot{B}_{17}+\dot{B}_{w,Pump3}+\dot{Y}_{Pump3}=\dot{B}_{18}$	-

$$\eta_{ex,winter}=\frac{\int\left(\dot{W}_{net}+\dot{E}x_{P,heatr}\right)d\tau}{\int\left(\dot{E}x_{AB}+\dot{E}x_{P,sun}\right)d\tau} \quad (33)$$

where Ex_{18} is the auxiliary boiler input exergy, which can be given as [46]:

$$\dot{E}x_{AB}=\dot{m}_{NG}\times LHV \quad (34)$$

In Eq. (32), $Ex_{P,Sun}$ is the solar input exergy to the system, which can be expressed as [47]:

$$Ex_{p,sun}=G_tA_{PTC}\left[1+\frac{1}{3}\left(\frac{T_0}{T_{sun}}\right)^4-\frac{4}{3}\left(\frac{T_0}{T_{sun}}\right)\right] \quad (35)$$

In Eq. (35), T_{sun} is the temperature of the sun, which is given to be 6,000 K (47).

4.2.Total product cost rate

The total product cost rate of the overall system, $C_{P,tot}$ is defined as the sum of the product cost rates of the turbine and the evaporator in summer, and the turbine and the heater in winter:

$$\dot{C}_{P,tot,summer}=\dot{C}_{P,Evap}+\dot{C}_{Tur} \quad (36)$$

$$\dot{C}_{P,tot,winter}=\dot{C}_{P,heater}+\dot{C}_{Tur} \quad (37)$$

Table 2-b. Exergo-environmental balances and auxiliary equations for the system components in winter

Components	Exergo-environmental balance equations	Auxiliary equations
The CCHP subsystem		
Vapour generator	$\dot{B}_1+\dot{B}_{13}+\dot{Y}_{VG}=\dot{B}_2+\dot{B}_{14}$	$b_{13}=b_{14}$
Separator	$\dot{B}_2+\dot{Y}_{Sep}=\dot{B}_3+\dot{B}_4$	$\frac{\dot{B}_4-\dot{B}_2}{\dot{E}x_4-\dot{E}x_2}=\frac{\dot{B}_3-\dot{B}_2}{\dot{E}x_3-\dot{E}x_2}$
Turbine	$\dot{B}_3+\dot{Y}_{Tur}=\dot{B}_{21}+\dot{B}_5+\dot{B}_{w,Tur}$	$b_3=b_5=b_{21}$
HT Recuprator	$\dot{B}_4+\dot{B}_{11}+\dot{Y}_{HT}=\dot{B}_1+\dot{B}_6$	$b_1=b_{11}$
LT Recuprator	$\dot{B}_7+\dot{B}_{33}+\dot{Y}_{LT}=\dot{B}_8+\dot{B}_{11}$	$b_7=b_8$
Mixer1	$\dot{B}_5+\dot{B}_6+\dot{Y}_{Mxr1}=\dot{B}_7$	-
Pump1	$\dot{B}_9+\dot{B}_{w,Pump1}+\dot{Y}_{Pump1}=\dot{B}_{10}$	-
Mixer4	$\dot{B}_{10}+\dot{B}_{34}+\dot{Y}_{Mxr4}=\dot{B}_{33}$	-
Condenser	$\dot{B}_8+\dot{B}_{19}+\dot{Y}_{Con}=\dot{B}_9+\dot{B}_{20}$	$b_9=b_{23}$
Heater	$\dot{B}_{21}+\dot{B}_{35}+\dot{Y}_{heater}=\dot{B}_{36}+\dot{B}_{34}$	$b_{34}=b_{21}$
The solar collection subsystem		
Storage tank	$\dot{B}_{15}+\dot{B}_{16}+\dot{Y}_{ST}=\dot{B}_{17}+\dot{B}_{12}+\dot{B}_L$	$b_{12}=b_{17}$
Pump2	$\dot{B}_{14}+\dot{B}_{w,Pump2}+\dot{Y}_{Pump2}=\dot{B}_{15}$	-
Auxiliary boiler	$\dot{B}_{12}+\dot{B}_f+\dot{Y}_{AB}=\dot{B}_{13}$	-
PTC	$\dot{B}_{18}+\dot{B}_{sun}+\dot{Y}_{PTC}=\dot{B}_{16}$	-
Pump3	$\dot{B}_{17}+\dot{B}_{w,Pump3}+\dot{Y}_{Pump3}=\dot{B}_{18}$	-

4.3.Total product environmental impact rate

The total net output-related environmental impact rate for the overall system for each season is defined as follows:

$$\dot{B}_{P,tot,summer}=\dot{B}_{P,Evap}+\dot{B}_{Tur} \quad (38)$$

$$\dot{B}_{P,tot,winter}=\dot{B}_{P,heater}+\dot{B}_{Tur} \quad (39)$$

5.Results and Discussion

Exergy, exergo-economic, and exergo-environmental modelling of the system have been conducted based on the simulation code in the Engineering Equation Solver (EES) [48]. Table 4 lists the main input, thermodynamic parameters for the simulation of the desired CCHP system.

Table 5 indicates the simulation results of the desired system for both seasons. It is revealed that the daily energy efficiencies in summer and winter are 5.53% and 36.82% respectively, and the daily exergy efficiencies are 4.15% and 33.05% respectively. The significant difference between the efficiencies of both seasons stems from the differences in the input energies and exergies. In summer, the solar fraction is higher than that in winter. That is because in summer, the desired system employs higher solar radiation in comparison with winter. Therefore, the mass flow rate of fuel increases in winter.

Applying the ejector in the refrigeration cycle to produce a cooling load in summer causes an increment in the total product cost rate of the system in comparison with winter.

That is because the product cost rate of the heat exchanger to produce the heat load in winter is lower than that of the ejector in summer. Furthermore, the lower output power in winter compared with the summer mode leads to a decrease in the power cost rate in winter. The results indicate that in winter, the output power decreases, causing a decrease in the environmental impact associated with the lifecycle of all components (Y_{tot}). Moreover, the exergy destruction of the heat exchanger in winter is lower than the exergy destruction of the ejector in summer. These reasons lead to a fall in the total product environmental impact in winter compared with summer.

Table 3. Simulation conditions for the CCHP system

Term	**Summer**	**Winter**
Environmental condition		
Simulation date	June 11	Des 10
Dead state temperature, T0 (K)	278	278
Dead state pressure, P0 (bar)	1	1
CCHP subsystem		
System inlet mass flow rate, m_1 (kg/s)	16.8	16.8
System inlet concentration of ammonia (kg/kg)	0.82	0.82
Pressure drop of ejector, Δp (bar)	0.1	-
Pressure ratio of ejector, PLR	3.5	-
Turbine outlet pressure, P5 (bar)	6.6	6.6
Turbine inlet pressure, P3 (bar)	33.3	33.3
Turbine extraction pressure, P21 (bar)	13	13
Turbine inlet temperature, T3 (K)	389	387
Therminol flow rate in storage cycle, m_{13} (kg/s)	170	170
Water flow rate at evaporator, m_{28} (kg/s)	5	-
Heater inlet temperature, T35 (K)	-	278
Condenser temperature T19 (K)	278	278
Maximum cycle temperature T13 (K)	395	393
Pinch point temperature difference in vapour generator, PP (K)	6	6
Pinch point temperature difference in HT& LT recuperators, PP (K)	5	5
Pinch point temperature difference in condenser, PP (K)	3	3
Turbine isentropic efficiency	80%	80%
Pumps isentropic efficiency	80%	80%
Collector subsystem		
Collector flow rate, m_{18} (kg/s)	200	200
Auxiliary boiler efficiency	80%	80%
Lower heating value of fuel (kJ/kg)	51,292	51,292
Storage tank numbers	10	10
Overall coefficient of storage tank U (W/m2 K)	0.0018	0.0018
Area of storage tank A (m2)	28	28
Volume of storage tank (m3)	10	10

Table 4. The thermodynamic performance simulation for the CCHP system

Term	**summer**	**winter**
Daily thermal efficiency, η_{th} (%)	5.53	36.82
Daily exergy efficiency, η_{ex} (%)	4.147	33.05
Total product of environment impact, $\dot{B}_{P,tot}$ (Pts/s)	0.1791	0.1326
Total product cost rate, $\dot{C}_{P,tot}$ ($/s)	1.696	1.096
Total product exergy, $\dot{E}x_{P,tot}$ (kW)	3845	2195
System inlet energy, $\dot{E}_{in}$ (kW)	26365.75	24225.79
Total fuel environment impact, $\dot{B}_{F,tot}$ (Pts/s)	0.09543	0.1122
System inlet exergy, $\dot{E}x_{in}$ (kW)	33224	26668
Total fuel cost rate, $\dot{C}_{F,tot}$ ($/s)	0.01809	0.02127
Total output energies, $\dot{W}_{net}+\dot{Q}_{Heating}+\dot{Q}_{Cooling}$, (kW)	1740.15	8817

6.Optimization results

The NSGA-II method is employed to find the optimum performance of the desired system for all working fluids for both summer and winter. Six key parameters, namely, the mass flow rate of the mixture in the vapour generator, the turbine inlet pressure, the turbine outlet pressure, the turbine extraction pressure, the pinch temperature difference of the vapour generator, and the pressure drop of the ejector, were chosen as the decision variables in summer. Five main parameters, namely, mass flow rate of a mixture in the vapour generator, the turbine inlet pressure, the turbine outlet pressure, the turbine extraction pressure, and the pinch temperature difference of the vapour generator, were chosen as the decision variables for winter. Table 6 lists the ranges of the decision variables for the optimization of various working fluids.

The optimization of energy systems is usually done by selecting more than one objective function. Often, the objective functions are conflicting. In this work, the optimization is done for three objective functions, including the daily exergy efficiency, the total product cost rate, and the total product environmental impact rate associated with exergy for each season, i.e. Eqs. 32, 36, and 38 for summer, and Eqs. 33, 37, and 39 for winter respectively.

In the desired system, two single objective optimizations are done for both seasons. In single optimization, only one special criterion can be optimized. In it, other criteria may not achieve their optimal values. Table 7 shows the optimum system performance and the corresponding combination of the decision variables.

According to Table 7, in single-objective optimization, the maximum daily exergy efficiency for summer is calculated as 4.275%, which indicates 3.09% increment compared with the base point. In this case, the minimum turbine outlet pressure with a value of 6.3 (bar) and the low value of the ejector pressure drop are required. The minimization of the total product cost rate leads to 24.88% improvement in comparison with the base case. The outcomes express that the minimum ejector pressure drop and the turbine inlet pressure with values of 0.05 (bar) and 32 (bar) respectively are needed in this case. Finally, minimizing the total product environmental impact rate improves the environmental impact of products within 13.4%. In this case, the minimum values of the mass flow rate of a mixture in the vapour generator, the turbine extraction pressure, and the pinch temperature difference of vapour generator are required.

It is observed that in winter, the maximum daily exergy efficiency with 38.25% increment relative to the base point is 45.69%. Optimization results indicate that the maximum daily exergy efficiency is achieved in minimum ranges of the mass flow rate, the turbine inlet pressure, the turbine extraction pressure, and the turbine outlet pressure with

Table 6. Data of the parameter optimization

Term	Summer	Winter
Mass flow rate of mixture in vapour generator, m_1 (kg/s)	16.8-17	16.5-20
Turbine inlet pressure, P3 (bar)	32-33.2	30-34
Turbine outlet pressure, P5 (bar)	6.3-6.6	6.5-8
Turbine extraction pressure, P21 (bar)	12.2-13.2	11-15
Pinch temperature difference of vapour generator, PP (K)	5-7	3-8
Pressure drop of ejector, ΔP (bar)	0.05-0.5	-

Table 5. Single-objective optimization

	Summer				Winter			
Term	**Base case**	**Max. η_{ex}**	**Min. $\dot{C}_{P,tot}$**	**Min. $\dot{B}_{P,tot}$**	**Base case**	**Max. η_{ex}**	**Min. $\dot{C}_{P,tot}$**	**Min. $\dot{B}_{P,tot}$**
Daily exergy efficiency, η_{ex} (%)	4.147	4.275	4.236	4.095	33.05	45.69	17.71	17.57
Total product cost, $C_{P,tot}$ ($/s)	1.696	1.662	1.274	1.823	1.096	1.062	0.5302	0.5395
Total product environment impact, $B_{P,tot}$ (Pts/s)	0.1791	0.1778	0.1806	0.1551	0.1326	0.1324	0.06441	0.0647
Pressure drop of ejector, ΔP (bar)	0.1	0.06	0.05	0.1	-	-	-	-
Mass flow rate of vapour generator, m_1 (kg/s)	16.8	16.83	16.9	16.8	16.8	16.5	19.97	20
Turbine inlet pressure, P3 (bar)	33.3	32.26	32	33	33.3	30	30	30.08
Turbine outlet pressure, P5 (bar)	6.6	6.3	6.45	6.48	6.6	6.5	8	7.924
Turbine extraction pressure, P21 (bar)	13	12.67	12.44	12.2	13	11	14.98	13.98
Pinch temperature difference of vapour generator, PP (K)	6	6.41	5.72	5	6	5.035	4.83	6.658

values of 16.5 kg/s, 30 bar, 11 bar, and 30 bar respectively.

The minimum total product cost rate is calculated as 0.5302 $/s, which shows a 51.62% improvement relative to the base point. This value is achieved when the value of the turbine inlet pressure is minimal, while high values of mass flow rate of the mixture in the vapour generator, turbine extraction and outlet pressure are needed. Minimizing the total product environmental impact rate depicts the value of 0.0647Pts/s, which shows a 51.21% improvement of environmental impact compared with the base case. At this point, high values of mass flow rate and turbine outlet pressure, at 20 kg/s and 7.974 bar respectively, are needed.

In this study, NSGA-II is employed to conduct the multi-objective optimization of a desired system to find the optimal conditions.

Figures 2 (a) and 3 (a) indicate the three dimensional (3D) Pareto optimal frontier for each season of multi-objective optimization. In addition, to illustrate the results of multi-objective optimization with two objective functions, three two dimensional (2D) diagrams, i.e. Figs. 2 (b-d) and 3 (b-d), in which the relation between two out of three objectives are clarified, are plotted.

Choosing a convenient optimum point from the obtained points on the Pareto frontier (Figs. 2 and 3) requires a decision-making process [49].

The final decision-making process is usually performed by considering an ideal point. If three criteria were individually optimized, the combination of these values would express the ideal point or the ideal criterion point. Since the ideal point is not often a solution located on the Pareto frontier, the existing points on the Pareto frontier closest to the ideal point might be considered as the final optimum solution. Before that, the criteria should be non-dimensionalized. In this paper, the LINMAP method is applied to non-dimensionalize the criteria using the relations in Ref. [49].

The final value of the optimum criteria, i.e. the daily exergy efficiency, the total product environmental impact rate, and the total product cost with corresponding design parameters using the above procedure are obtained for each season and listed in Table 8. Furthermore, these optimum points for each working fluid are marked in red in Figs. 2 and 3.

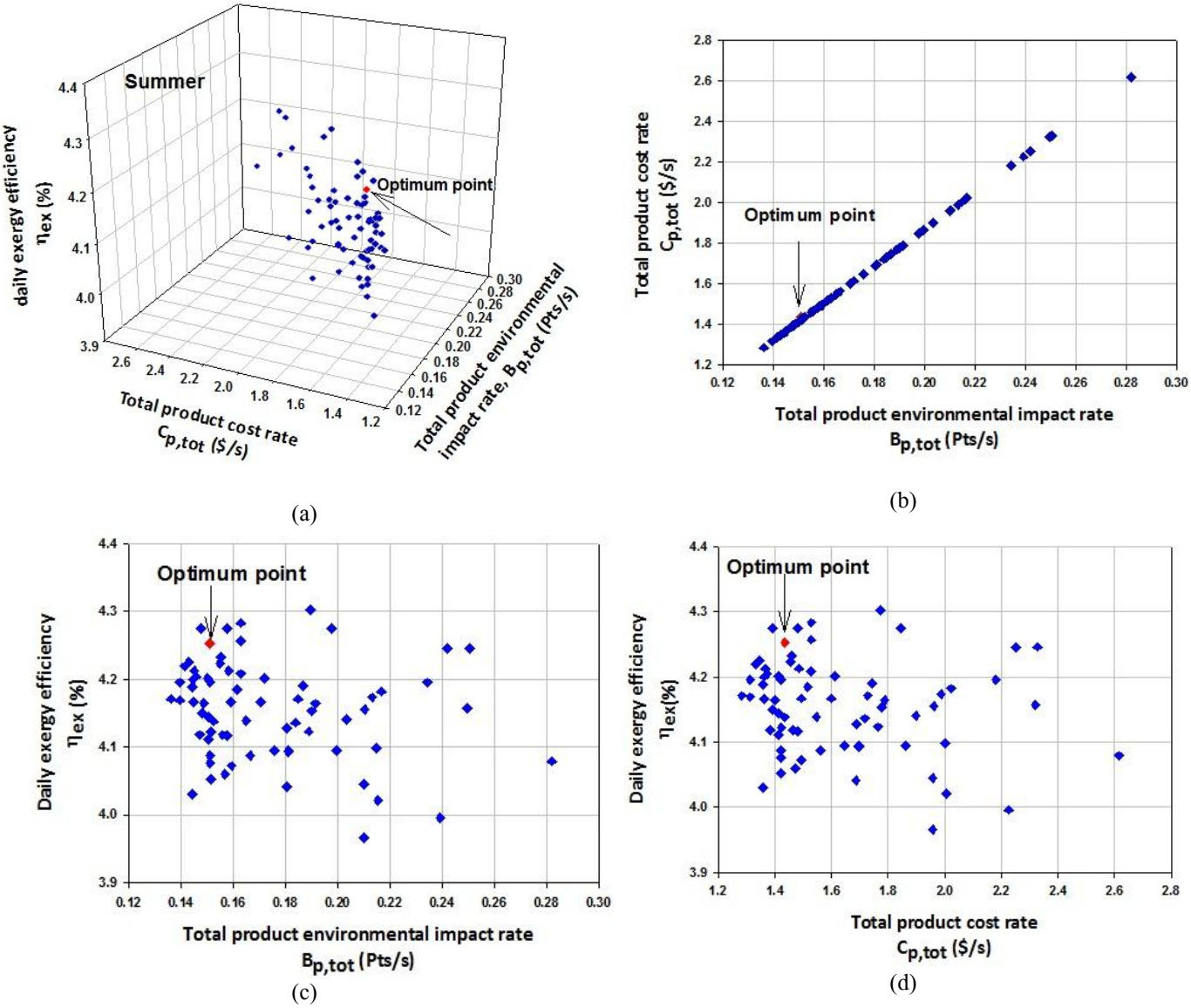

Fig. 2. Pareto optimal frontier (a) 3D and (b-d) 2D for summer

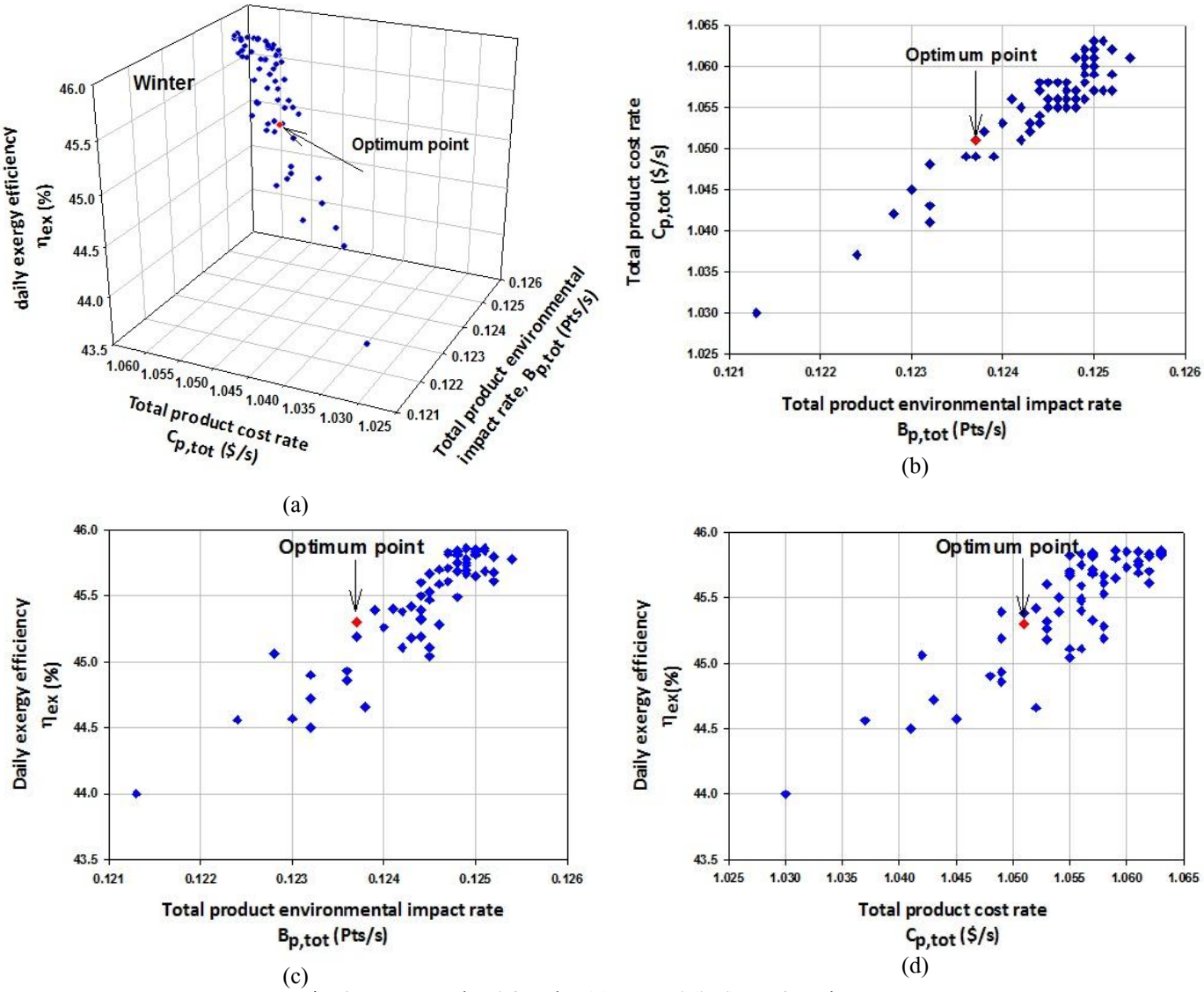

Fig. 3. Pareto optimal frontier (a) 3D and (b-d) 2D for winter

According to Table 8, in summer, 2.56%, 15.3%, and 15.7% improvements can be achieved for the daily exergy efficiency, the total product cost rate, and the total product environmental impact rate respectively, each relative to the base point. Comparing the optimization results indicates that the optimum values of daily exergy efficiency and the total product environmental impact rate decrease within 0.51% and 2.64% respectively. The total product cost rate increases within 21.18% in multi-objective optimization as compared with their single objective optimization.

At this point, the values of turbine inlet, outlet, and extraction pressures decrease by 3.9%, 1.82%, and 6.15% respectively relative to the base case. Furthermore, it is found that a minimum mass flow rate and pinch point with values of 16.8 kg/s and 5K respectively are required.

In winter, the daily exergy efficiency, the total product cost rate, and the total environmental impact rate improve by about 36.34%, 4.93%, and 7.39% respectively compared with the base point. The optimum value of the daily exergy efficiency decreases by 26.33%, and the total product cost rate and the total environmental impact rate increase by 97.66% and 93.35% respectively compared with their single objective optimization. Outcomes indicate that the values of mass flow rate and turbine inlet pressure obtained in multi-objective optimization are close to the lower values of their ranges while the value of turbine outlet pressure is close to the higher value of its range.

Table 6. Multi-objective optimization

Optimum point in multi-objective optimization	**Summer**	**Winter**
Daily exergy efficiency, η_{ex} (%)	4.253	33.66
Total product cost, $\dot{C}_{P,tot}$ ($/s)	1.436	1.048
Total product environment, $\dot{B}_{P,tot}$ (Pts/s)	0.151	0.1251
Pressure drop of ejector, ΔP (kPa)	0.05	-
Mass flow rate of mixture in vapour generator, $\dot{m}_1$ (kg/s)	16.8	16.51
Turbine inlet pressure, P3 (bar)	32	30.14
Turbine outlet pressure, P5 (bar)	6.48	7.719
Turbine extraction pressure, P21 (bar)	12.2	13.95
Pinch temperature difference of vapour generator, PP (K)	5	6.767

Figure 4 depicts the distribution of the mass flow rate for the Pareto frontier in its design range for summer (Fig. 4-a) and winter (Fig. 4-b) respectively. It is clear that the optimum solutions of mass flow rate in summer is located in the range of 6.8–17 kg/s, while in winter, the solutions are close to 16.5 kg/s. In summer, as the mass flow rate increases, the daily exergy efficiency rises strongly due to the increment of output power while the total product cost rate ($\dot{C}_{tot}$) and the total environmental impact rate decrease slightly. That is because not only do the total investment cost rate and the environmental impact rate associated with the lifecycle assessment of all components ($\dot{Y}_{tot}$) decrease, the exergy destruction of the ejector falls as well. Therefore, every value of the mass flow rate can be the optimum value in the optimization. In winter, an increment in mass flow rate leads to a slight increase in output power and a significant fall in the heat load produced in the heat exchanger. Therefore, the daily exergy efficiency strongly deceases while the total product cost rate and the total product environmental impact rate decrease slightly. In this case, the low values of mass flow rate give better optimum solutions compared with the high values.

Figure 5 indicates the distribution of the turbine inlet pressure for the Pareto frontier in summer (Fig. 5-a) and in winter (Fig. 5-b). The optimum turbine inlet pressure in summer is located across the design range. In winter, it is located in the range of the 30–31.5 bar. According to Fig. 5-a, in summer, the increment of turbine inlet pressure has a positive effect on the performance of the desired system so that the output power increases, and the total exergy destruction of

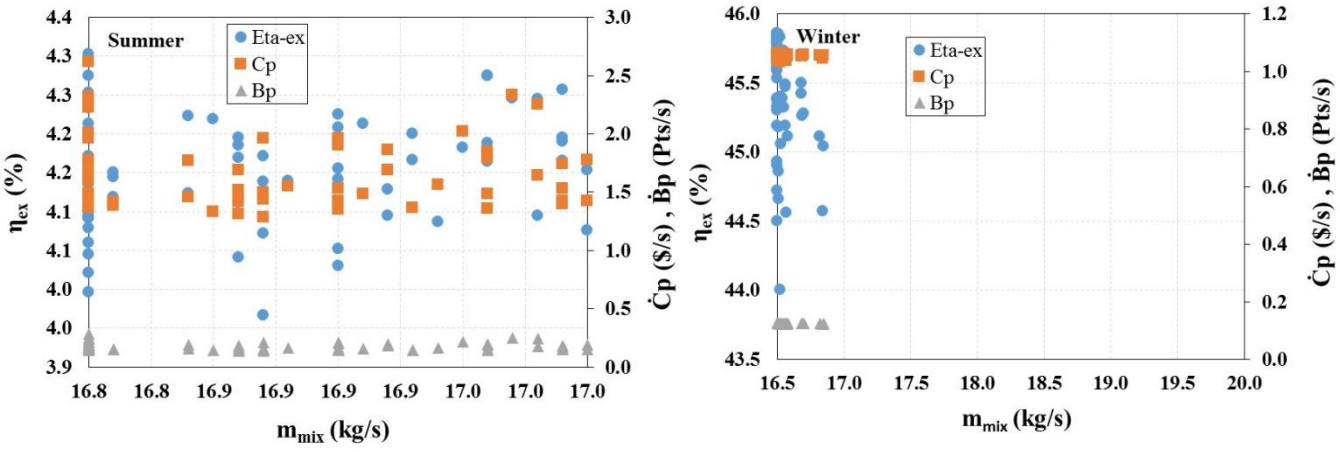

(a) (b)

Fig. 4. Distribution of mass flow rate for the Pareto frontier in its design range (a) in summer and (b) in winter modes

the system decreases. These changes lead to an increase in the daily exergy efficiency and a decrease in the total product cost rate as well as the total product environmental impact rate. As Fig. 5-b illustrates, the produced heating load decreases significantly as turbine inlet pressure rises in winter, causing a strong decrease in daily exergy efficiency. On the other hand, the total product cost rate and the total product environmental impact rate of the system remain almost the same as the turbine inlet pressure increases. Therefore, the low values of turbine inlet pressure provide better performance of the system.

Figure 6 illustrates the distribution of turbine back pressure for the Pareto frontier in summer (Fig. 4-a) and winter (Fig. 4-b). According to Fig. 6-a, the optimum values of turbine back pressure in summer are almost located across the design range. It is clear that the accumulation of points for the optimal daily exergy efficiency is close to the 6.3 bar. That is because in summer, the increment of turbine back pressure decreases the output power, which causes a significant decrease in the daily exergy efficiency of the system. The decrease in output power has a slight positive effect on the total product cost rate and the total product environmental impact rate of the system. As Fig. 6-b illustrates, the accumulation of the optimum turbine back pressure values are close to the 6.5–7.5 bar. That is because in winter, as the turbine back pressure increases, the temperature goes up,

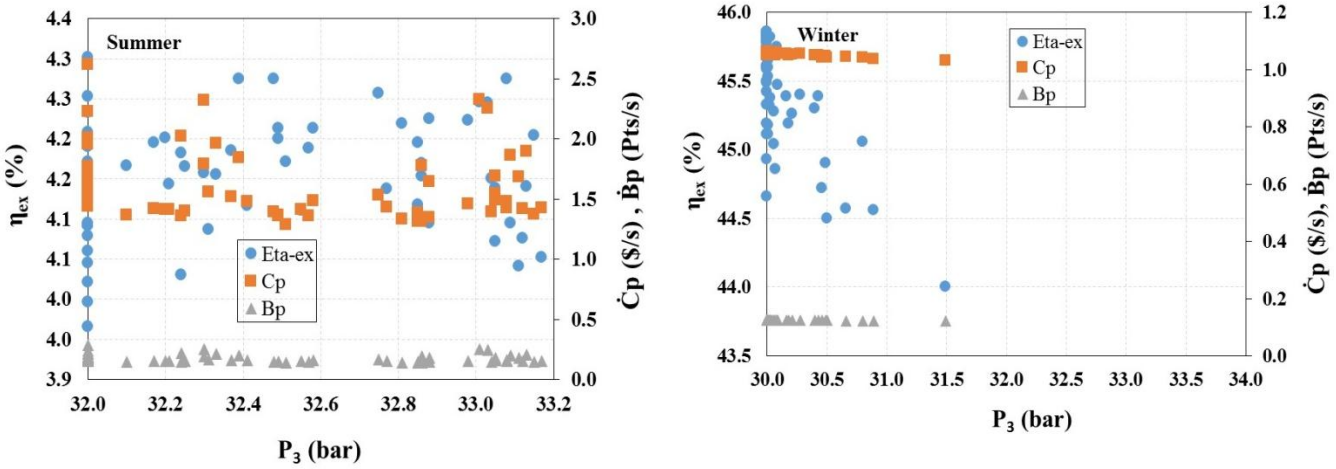

(a) (b)

Fig. 5. Distribution of turbine inlet pressure for the Pareto frontier in its design range in (a) summer and (b) winter modes

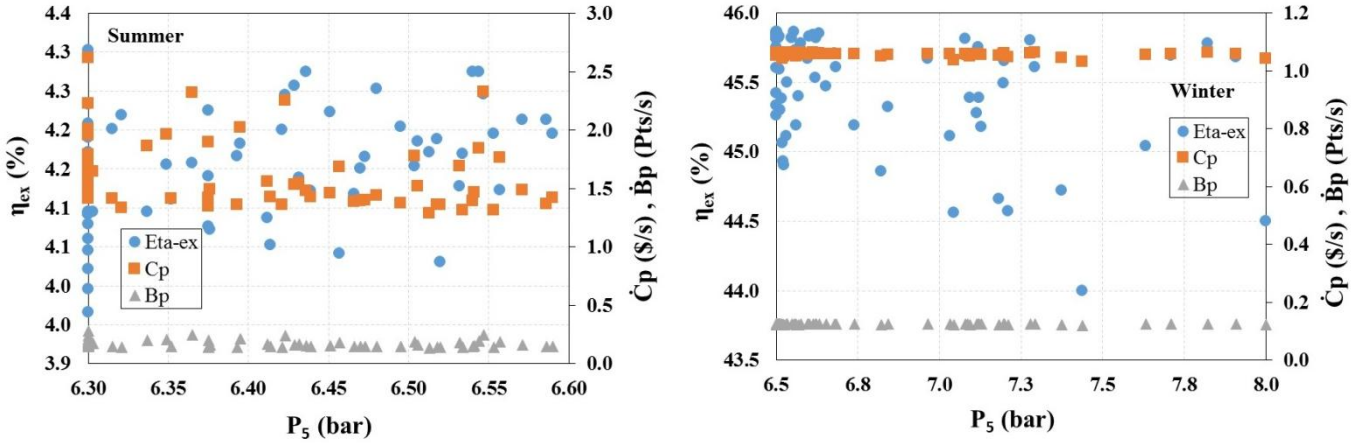

(a) (b)

Fig. 6. Distribution of turbine back pressure for the Pareto frontier in its design range (a) in summer and (b) in winter modes

and thus, the enthalpy of point 21 rises, which leads to a significant increase in the produced heating load. Therefore, the daily exergy efficiency of the system increases. Meanwhile, the total product cost rate and the total product environmental impact rate increase because of the increment of the total investment cost rate ($\dot{Z}_{tot}$) as well as the total environmental impact rate associated with lifecycle assessment of all components ($\dot{Y}_{tot}$). These changes provide a specific range for the optimum turbine back pressure.

Figure 7 illustrates the distribution of the turbine extraction pressure for the Pareto frontier for summer (Fig. 7-a) and for winter (Fig. 7-a). As shown in Fig. 7-a, in summer, the optimum turbine extraction pressure for the daily exergy efficiency and the total product cost rate are concentrated close to the low value of the design range. For the total product environmental impact rate, it is located across the design range. The output power significantly decreases and the total exergy destruction of the system increases due to the high exergy destruction of the ejector as turbine extraction pressure rises. These variations cause a strong decrease in the daily exergy efficiency and an increase in the total product cost rate. Therefore, the optimum solution for these criteria is located in the low values of the design range. On the other hand, the total product environmental impact rate increases slightly as the turbine extraction pressure rises. According to Fig. 7-b, the optimum turbine extraction pressure is located in the design range. In winter, an increase in turbine extraction pressure does not have any significant effect on the desired criteria so that all objective functions remain almost constant as the turbine extraction pressure increases. Therefore, the optimum solution is distributed in the design range.

Figure 8 illustrates the distribution of the pinch temperature difference of vapour generator for the Pareto frontier for summer (Fig. 8-a) and winter (Fig. 8-b). In summer, the optimum pinch temperature difference of the vapour generator is concentrated in the range of 5–6 K. In summer, the increment of the pinch temperature difference of the vapour generator has a negative effect on each criterion because the output power and the product cost rate of the ejector increase as pinch temperature rises. Therefore, the daily exergy efficiency decreases and the total product cost rate increases significantly. On the other hand, the increment of the product environmental impact of the ejector leads to an increase in the total product environmental impact rate of the system as the pinch temperature difference increases. According to Fig. 8-b, in winter, the optimum pinch temperature difference of the vapour generator is located in the range of 4.5–7 K. The increment of the pinch temperature difference has only a positive effect on the daily exergy efficiency due to an increase in the produced heating load in the heat exchanger, but it has a negative effect on both the total product cost rate and the total product environmental impact rate of the system owing to an increment of $\dot{Z}_{tot}$ and $\dot{Y}_{tot}$ respectively.

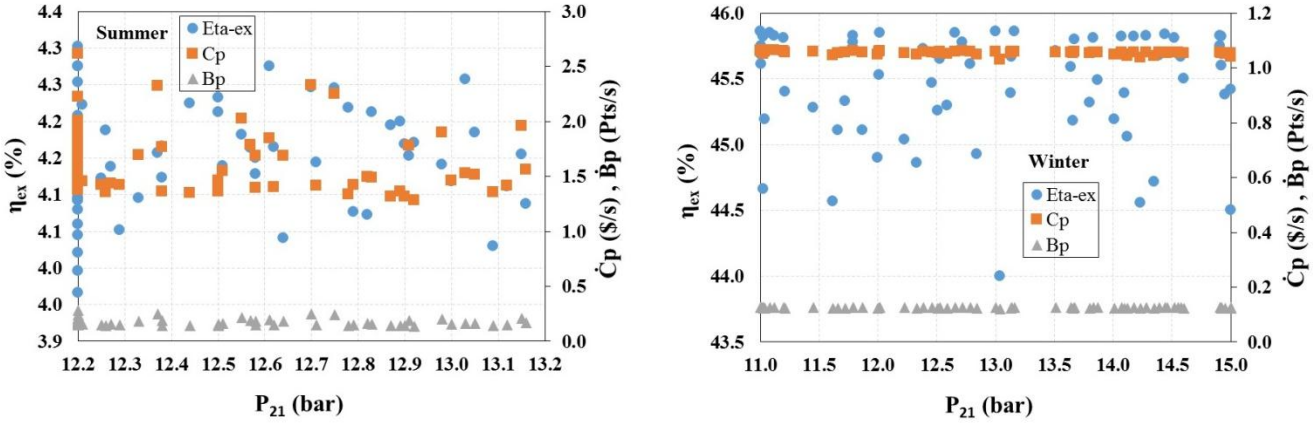

(a) (b)

Fig. 7. Distribution of turbine extraction pressure for the Pareto frontier in its design range (a) in summer and (b) in winter modes

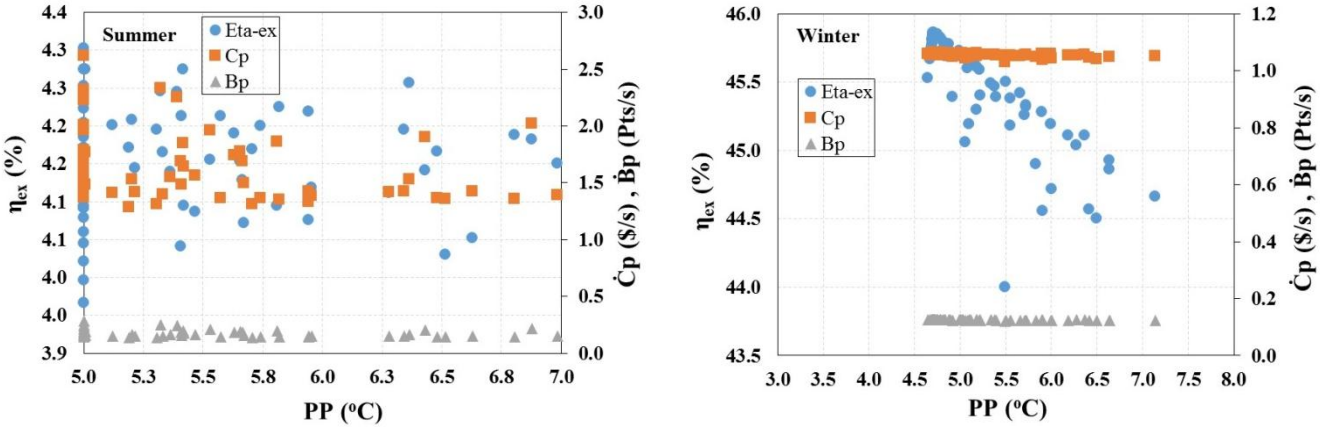

(a) (b)

Fig. 8. Distribution of the pinch temperature difference of vapour generator for the Pareto frontier in its design range (a) in summer and (b) in winter modes

Figure 9 depicts the distribution of the ejector pressure loss for the Pareto frontier in summer. It is clear that the optimum ejector pressure loss is located in the range across the design range. In this case, the net output of the system remains constant as the ejector pressure loss increases. Therefore, the daily exergy efficiency does not change. On the other hand, the values of $\dot{C}_{tot}$ and $\dot{Y}_{tot}$ fall slightly while the total fuel cost rate and the total fuel environmental impact rate remain almost constant. These changes lead to a slight decrease in the total product cost rate and the total product environmental impact rate.

7. Conclusion

The present work modelled and evaluated a new solar CCHP Kalina cycle using exergy, exergo-economic, and exergo-environmental approaches. The daily exergy efficiency, the product cost rate, and the total product environmental impact rate were then optimized simultaneously for both summer and winter. The main conclusions arising from the present study are summarized as follows:

- The values of the total product environmental impact and cost rates calculated for the winter cycle are lower than those in the summer cycle while the daily exergy efficiency of the winter cycle is higher than that of the summer cycle.
- In summer, the simultaneous increment of the turbine inlet pressure and the mass flow rate of the vapour generator have a positive effect on all criteria.
- In winter, the increment of turbine outlet pressure increases the daily exergy efficiency significantly while the total environmental impact and the cost rates of products fall as the turbine inlet and extraction pressures and the mass flow rate of the vapour generator rise.
- The optimization of the summer cycle improves the total product environmental impact and cost rates within 15.7% and 15.3% respectively.
- The optimization result of the winter cycle indicates 7.39% and 4.93% improvements for the total product environmental impact and cost rates respectively.

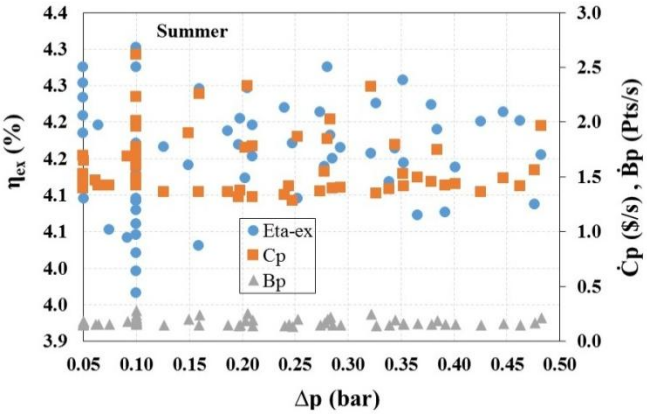

Fig. 9. Distribution of the ejector pressure loss for the Pareto frontier in its design range in summer mode

References

[1] Kalina A.I., Generation of Energy by Means of a Working Fluid, and Regeneration of a Working Fluid (1982)

[2] Nag P.K., Gupta A.V.S.S.K.S., Exergy Analysis of the Kalian Cycle, Applied Thermal Engineering (1998) 427-439.

[3] Xinxin Z., Maogang H., Ying Z., A Review of Research on the Kalian Cycle, Renewable and Sustainable Energy Reviews (2012) 5309-5318.

[4] Kalina A., Leibowitz H., Application of the Kalina Cycle Technology to Geothermal Power Generation, Geothermal Resources Council Transactions (1989)p. 11-605.

[5] Hettiarachchi H., Golubovic M., Worek W., The Performance of the Kalina Cycle System 11 (KCS-11) with Low-Temperature Heat Sources, Journal Energy Resour Techno (2007) 243-247.

[6] Nasruddin, et al., Energy and Exergy Analysis of Kalina Cycle System (KCS) 34 with Mass Fraction Ammonia-Water Mixture Variation, Mechanical Science and Technology (2009)1871-1876.

[7] Lolos P.A., Rogdakis E.D., Thermodynamic Analysis Of A Kalina Power Unit Driven By Low Temperature Heat Sources. Thermal science (2009) 13: 21-31.

[8] Sun F., Ikegami Y., Jia B., A Study on Kalina Solar System with an Auxiliary Superheater, Renewable Energy (2012) 41: 210-219.

[9] Shankar Ganesh N., Srinivas T., Optimized Kalina Cycle, in Frontiers in Automobile and Mechanical Engineering (FAME)(2010).

[10] Wang J., et al., Parametric Analysis and Optimization of a Kalina Cycle Driven by Solar Energy. Applied Thermal Engineering (2013)50(1): 408-415.

[11] Li X., Zhang Q., Li,X., A Kalina Cycle with Ejector, Energy (2013) 54(0): 212-219.

[12] Xu F., Yogi Goswami D., Bhagwat S. S., A Combined Power/Cooling Cycle. Energy (2000) 25(3): 233-246.

[13] Tamm G., et al., Theoretical and Experimental Investigation of an Ammonia–Water Power and Refrigeration Thermodynamic Cycle, Solar Energy (2004) 76(1): p. 217-228.

[14] Martin C., Goswami D.Y., Effectiveness of Cooling Production with a Combined Power and Cooling Thermodynamic Cycle, Applied Thermal Engineering, (2006) 26(5–6): 576-582.

[15] Padilla R.V., et al., Analysis of Power and Cooling Cogeneration Using Ammonia-Water Mixture, Energy (2010) 35(12): 4649-4657.

[16] Demirkaya G., et al., Analysis of a Combined Power and Cooling Cycle for Low-Grade Heat Sources, Energy Research (2010) 35: 1145-1157.

[17] Jawahar C., et al., Simulation Studies on Gax Based Kalina Cycle for Both Power and Cooling Applications, Applied Thermal Engineering (2011).

[18] Zare V., et al., Thermoeconomic Analysis and Optimization of an Ammonia–Water Power/Cooling Cogeneration Cycle,Energy (2012).

[19] Ma S., et al., Thermodynamic Analysis of a New Combined Cooling, Heat and Power System Driven by Solid Oxide Fuel Cell Based on Ammonia–Water Mixture, Journal of Power Sources, (2011) 196(20): 8463-8471.

[20] Meyer L., et al., Exergoenvironmental Analysis for Evaluation of the Environmental Impact of Energy Conversion Systems, Energy(2009) 34(1): 75-89.

[21] Boyano A., et al., Exergoenvironmental Analysis of a Steam Methane Reforming Process for Hydrogen Production, Energy (2011) 36(4): 2202-2214.

[22] Petrakopoulou F., et al., Exergoeconomic and Exergoenvironmental Analyses of a Combined Cycle Power Plant with Chemical Looping Technology, International Journal of Greenhouse Gas Control (2011)5(3): 475-482.

[23] Petrakopoulou F., et al., Exergoeconomic and Exergoenvironmental Evaluation of Power Plants Including CO 2 Capture, Chemical Engineering Research and Design (2011) 89(9): 1461-1469.

[24] Atılgan R., et al., Environmental Impact Assessment of a Turboprop Engine with the Aid of Exergy, Energy (2013) 58: 664-671.

[25] Abusoglu A., M.S. Sedeeq, Comparative Exergoenvironmental Analysis and Assessment of Various Residential Heating Systems, Energy and Buildings, (2013) 62: 268-277.

[26] Blanco-Marigorta A.M., Masi M., Manfrida G., Exergo-Environmental Analysis of a Reverse Osmosis Desalination Plant in Gran Canaria, Energy (2014)76: 223-232.

[27] Hamut H., Dincer I., Naterer G., Exergoenvironmental Analysis of Hybrid Electric Vehicle Thermal Management Systems, Journal of Cleaner Production (2014)67187-196.

[28] Khoshgoftar Manesh, M., et al., Exergoeconomic and Exergoenvironmental Evaluation of the Coupling of a Gas Fired Steam Power Plant with a Total Site Utility System. Energy Conversion and Management, (2014)77: 469-483.
[29] Keçebaş A., Exergoenvironmental Analysis for a Geothermal District Heating System, An Application, Energy, (2016)94: 391-400.
[30] Fergani Z., Touil D., Morosuk T., Multi-Criteria Exergy Based Optimization of an Organic Rankine Cycle for Waste Heat Recovery in the Cement Industry, Energy Conversion and Management (2016)112: 81-90.
[31] Mosaffa A., Farshi L.G., Exergoeconomic and Environmental Analyses of an Air Conditioning System Using Thermal Energy Storage, Applied Energy(2016) 162: 515-526.
[32] Kalogirou S.A., Solar Energy Engineering, Processes and Systems. (2009).
[33] Bejan A., Moran M.J., Thermal Design and Optimization (1996).
[34] Li. H., et al., Performance Characteristics of R1234yf Ejector-Expansion Refrigeration Cycle, Applied Energy, (2014)121: 96-103.
[35] Wang J., Dai Y., Sun Z., A Theoretical Study on a Novel Combined Power and Ejector Refrigeration Cycle, International Journal of Refrigeration (2009)32(6): 1186-1194.
[36] Çengel Y.A., Boles M.A., Thermodynamics: an Engineering Approach, McGraw-Hill Higher Education (2006).
[37] Ogriseck S., Integration of Kalina Cycle in a Combined Heat and Power Plant, A Case Study, Applied Thermal Engineering (2009) 29(14–15): 2843-2848.
[38] Index M.S.E.C., Economic Indicators. Chemical engineering, September (2013) 76.
[39] Ahmadi P., Dincer I., Rosen M.A., Multi-Objective Optimization of a Novel Solar-Based Multigeneration Energy System. Solar Energy (2014)108: 576-591.
[40] Smith R.M., Chemical Process, Design and Integration(2005).
[41] Zhou C., Doroodchi E., Moghtaderi B., An in-Depth Assessment of Hybrid Solar–Geothermal Power Generation, Energy Conversion and Management, (2013)74: 88-101.
[42] Campos Rodríguez C.E., et al., Exergetic and Economic Comparison of ORC and Kalina Cycle for Low Temperature Enhanced Geothermal System in Brazil, Applied Thermal Engineering (2012).
[43] El-Emam R.S., Dincer I., Exergy and Exergoeconomic Analyses and Optimization of Geothermal Organic Rankine Cycle, Applied Thermal Engineering(2013)59(1): 435-444.
[44] Petrakopoulou F., et al., Environmental Evaluation of a Power Plant Using Conventional and Advanced Exergy-Based Methods, Energy(2012)45(1): 23-30.
[45] Boyano A., et al., Exergoenvironmental Analysis of a Steam Methane Reforming Process for Hydrogen Production, Energy(2011)36(4): 2202-2214.
[46] Kanoglu, M., Bolatturk A., Performance and Parametric Investigation of a Binary Geothermal Power Plant by Exergy. Renewable Energy(2008) 33(11): 2366-2374.
[47] Van Gool W., Energy Policy, Fairy Tales and Factualities, in Innovation and Technology—Strategies and Policies, Springer (1997) 93-105.
[48] Solver., E.E.E., Available at: http://www.fchart.com/.
[49] P-L Y., Multiple-Criteria Decision Making, Concepts, Techniques, and Extensions, Springer Science & Business Media (2013).